*Journal of Marine Research, 48,* 471–504, 1990

# The evolution of salt fingers in inertial wave shear

by Eric Kunze[1]

## ABSTRACT

Shadowgraph profiles collected in the thermohaline staircase east of Barbados reveal nearly-horizontal banding—unlike the vertical banding that has been observed in other fingering-favorable parts of the ocean. A plausible interpretation of this optical microstructure is that vertical shear is tilting over fingers. This paper presents a model for shear-tilting of salt fingers. The $Ri = 6$ inertial wave shears observed in C-SALT would tilt over and damp out square planform ($k_x = k_y$) fingers so rapidly that they could not produce significant fluxes. Vertical sheets aligned with the shear ($k_y = 0$) would behave like unsheared fingers if the shear was steady but oceanic shear is predominantly near-inertial so turns with time. Therefore, an across-sheet shear component will develop and initially-aligned sheets too will ultimately be tilted over. This happens slowly enough that sheets can grow to produce significant fluxes. When the growth of tilting sheets is limited by a critical inverse finger Richardson number, $(\nabla \times V)^2/N^2 \sim 3$–16, the model produces microstructure and fluxes similar to those reported from C-SALT. However, this constraint does not explain the density ratio dependence in laboratory studies and numerical simulations. What constrains finger growth needs to be better understood.

## 1. Introduction

This paper examines the effect of vertical shear on salt fingers to try to explain the nearly-horizontal laminae observed with a shadowgraph profiler in the fingering-favorable thermohaline staircase east of Barbados (Kunze *et al.,* 1987). Gregg and Sanford (1989) reported 10-m Richardson numbers across the staircase interfaces of ~6.

Linden's (1974) laboratory experiments demonstrated that, in *steady* shear with $Ri \geq 6$, vertical salt sheets aligned with the shear are the preferred mode of instability. The horizontal wavenumber of these sheets was identical to the fastest-growing wavenumber. In light of this, Schmitt and Georgi (1982) interpreted vertical banding in shadowgraph images from fingering-favorable layers where the instrument's optical path was aligned with the shear as salt sheets.

However, shadowgraph images from the thermohaline staircase east of Barbados (C-SALT) revealed not vertical but nearly horizontal banding in the fingering-

1. School of Oceanography WB-10, University of Washington, Seattle, Washington, 98195, U.S.A.

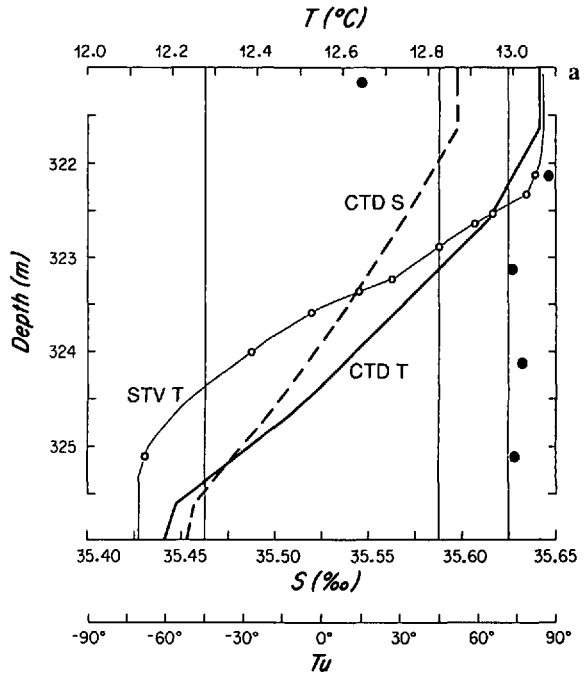


Figure 1. (a) Temperature and salinity profiles through a fingering-favorable interface in the thermohaline staircase east of Barbados. The interface is 3-m thick with a temperature step $\Delta T = 1°C$ and a salinity step $\Delta S = 0.15‰$ between two relatively well-mixed layers 10–20 m thick. The open circles on the higher-resolution STV temperature curve (thin solid curve) indicate the locations of the shadowgraph images shown in (b). Solid dots correspond to the Turner angle $Tu$ which is in the fingering regime ($Tu > 45°$) throughout the interface. (b) Shadowgraph images through a fingering-favorable interface (Fig. 1a). Each image is 10 cm in diameter and represents an average of the Laplacian of the index of refraction $\nabla^2\eta$ over the 60-cm long horizontal optical path. The upper left image from just above the top of the interface is optically quiet. Nearly-horizontal laminae with vertical wavelengths of 1 cm and tilts of 10–20° fill the images inside the interface. At these scales, the index of refraction should be almost entirely due to salt variance. Similar structure was found wherever gradients were fingering-favorable, and only where they were fingering-favorable.

favorable parts of the water column. Figure 1b shows a typical sequence of images through a fingering-favorable interface within the staircase (Fig. 1a). The interface is 3-m thick with differences $\Delta T = 1°C$, $\Delta S = 0.15‰$ across it. It is sandwiched between two well-mixed layers 10–20 m thick. Each shadowgraph image in Figure 1b is 10 cm in diameter and represents the Laplacian of the index of refraction, $\nabla^2\eta = a\nabla^2 T - b\nabla^2 S$, averaged over a 60-cm long horizontal optical path through seawater [$a = \partial\eta/\partial T$ and $b = \partial\eta/\partial S$ express the dependence of the index of refraction on temperature $T$ and salinity $S$; this dependence is roughly the same as that for

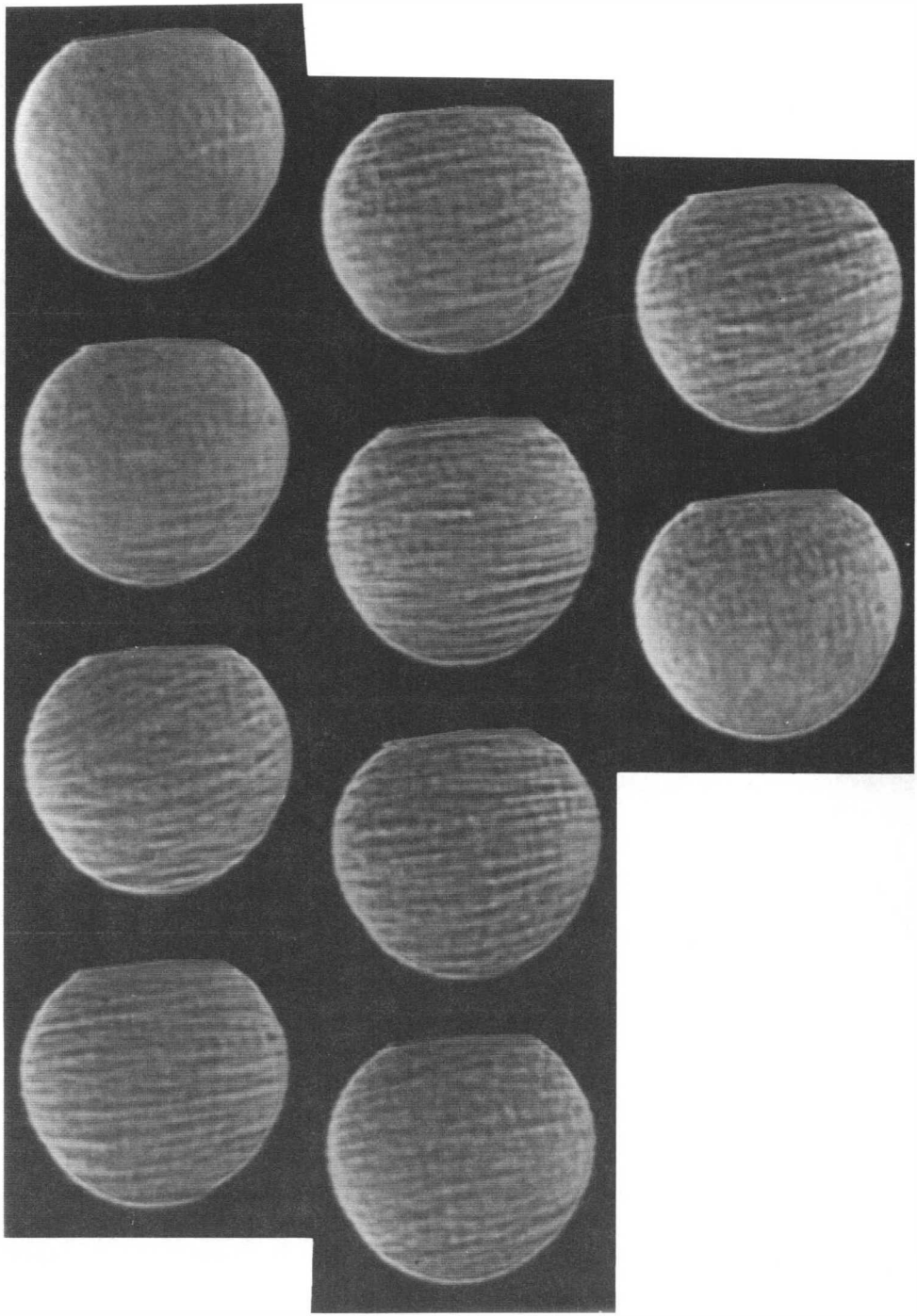

Figure 1b.

density]. The upper left image (Fig. 1b) is from above the interface and is optically quiet. The next image shows banding in its lower half.

The rest of the images, from within the interface, are filled with laminae. These nearly-horizontal striations have vertical wavelengths of 1 cm and are found not only in this interface, but wherever conditions favor fingering in the water column. Furthermore, laminae were not observed in the diffusively-stable parts of the profiles. The strong correlation between laminae and fingering-favorable conditions suggests that they are in some way connected with the salt-fingering form of double-diffusive instability. Other measurements provide evidence of plumes in the homogeneous layers (Marmorino *et al.*, 1987), pointing to double diffusion being an important source of mixing. Yet, of over 400 interfaces sampled with the shadowgraph profiler (Kunze *et al.*, 1987), there were no instances of the vertical banding that has been identified with salt-fingering in the laboratory (Turner, 1967; Shirtcliffe and Turner, 1970; Linden, 1973; Chen and Sandford, 1976) and in other fingering-favorable regions of the ocean (Williams, 1975, 1981; Schmitt and Georgi, 1982).

Kunze *et al.* (1987) suggested that the nearly horizontal banding observed in the staircase east of Barbados might be due either to fingers tilted over by vertical shear, or intrusive instabilities between Linden's (1974) salt sheets like those described by Holyer (1984). Two-dimensional numerical simulations (Shen, personal communication, 1990) show the potential for tilting by shear. Recent laboratory dye experiments by Nordeen Larson (personal communication, 1990) reveal that, while salt sheets develop in a steady shear, they break up into square planform fingers when the shear is turned off. If shear is then re-established, the fingers tilt over rather than re-forming sheets. Therefore, fingers cannot adjust their spatial structure to changing background shear.

Shear is dominantly near-inertial in the staircase east of Barbados (Fig. 2, Gregg and Sanford, 1987) as elsewhere in the ocean (Sanford, 1975; D'Asaro, 1984, 1985; Kunze *et al.*, 1990). So even if sheets were aligned initially, the inertially-rotating shear will produce an across-sheet component on a timescale of $f^{-1}$ (~8 h east of Barbados).

In this paper, the role of shear-tilting of fingers will be explored. The resulting model is used to try to simulate the C-SALT observations. To be convincing, it should be able to reproduce a number of unique features from the C-SALT measuements:

- the nearly-horizontal banding in shadowgraph images from the fingering-favorable parts of the profile (Kunze *et al.*, 1987) with *vertical* wavelengths of ~1 cm and *horizontal* wavelengths of ~6 cm.

- dominant *vertical* wavelengths in *temperature* microstructure of ~6 cm (Gregg and Sanford, 1987). The discrepancy in vertical scales between the shadowgraph and profiles may be because the shadowgraph measures the Laplacian of the index of refraction. The second derivative emphasizes the smallest scales and these are

likely to be due to salt because of its small diffusivity; temperature microstructure on 1-cm wavelengths would decay in only 25 s compared to 1 h for salt.

- dominant *horizontal* wavelengths in temperature microstructure of ~5–7 cm (Marmorino *et al.*, 1987; Lueck, 1987). These values are consistent with the fastest-growing wavelength (~3 cm; Stern, 1960; Schmitt, 1979b; Kunze, 1987) when account is taken for the random orientation of the tows with respect to sheets or fingers.

- average *layer* turbulent dissipation rates of $\sim 1.4 \times 10^{-10}$ W/kg, a factor of ~30 below those predicted by the laboratory-derived $\Delta S^{4/3}$ flux laws (Gregg and Sanford, 1987; Lueck, 1987) assuming the buoyancy-flux is balanced by dissipation in the layers $F_b = \epsilon$ (Businger *et al.*, 1971; Shay and Gregg, 1986). The $\Delta S^{4/3}$ flux law has been found to hold in the laboratory (Turner, 1967; Linden, 1973; Schmitt, 1979a; McDougall and Taylor, 1984), however, Kunze (1987) showed that it will only apply if the interface thickness is identical to a maximum finger length (~30 cm) as constrained by a critical finger Richardson or Stern number $(\nabla_H w)^2/N^2 = F_b/N^2 \sim 4$. Interfaces in the staircase east of Barbados were an order of magnitude too thick for individual fingers to extend through them.

- average *interface* dissipation rates of $\sim 5 \times 10^{-10}$ W/kg (Gregg and Sanford, 1987). These are higher than those in the layers but Gregg and Sanford caution that they may be biased high by temperature microstructure in the high-gradient interfaces.

- median interface Cox numbers (normalized by interface gradients) of ~10 (Lueck, 1987; Gregg and Sanford, 1987; Marmorino *et al.*, 1987).

One of the striking features in the C-SALT CTD data set is the near-constant *layer density ratio* in the staircase, $R_{\rho L} = \alpha \Delta T/\beta \Delta S = 0.85 \pm 0.02$ (Schmitt *et al.*, 1987). Using a one-dimensional advective-diffusive balance, Schmitt (1988) argued that the layer density ratio should be identical to the flux ratio through the interfaces. However, McDougall (1990) shows that these two quantities *cannot* be identical due to the nonlinearity of the equation of state (see Appendix A). He finds that very weak interfacial advection $w_i$ (with $R_F = R_\rho = 1.6$) coupled with fingering/molecular diffusion ($R_F < 1$) could account for the layer density ratio. Since the layer density ratio does not necessarily constrain the flux ratio, it cannot be compared to the model's flux ratio.

## 2. Equations of motion

The basic assumptions of the model are sketched in Figure 2. The model is similar to that described by Kunze (1987) except that it allows for tilted fingers. The upper panel of Figure 2a represents a vertical slice through a zone of fingers or sheets. The fingers consist of alternating finite-length columns of up- and downflowing fluid embedded in

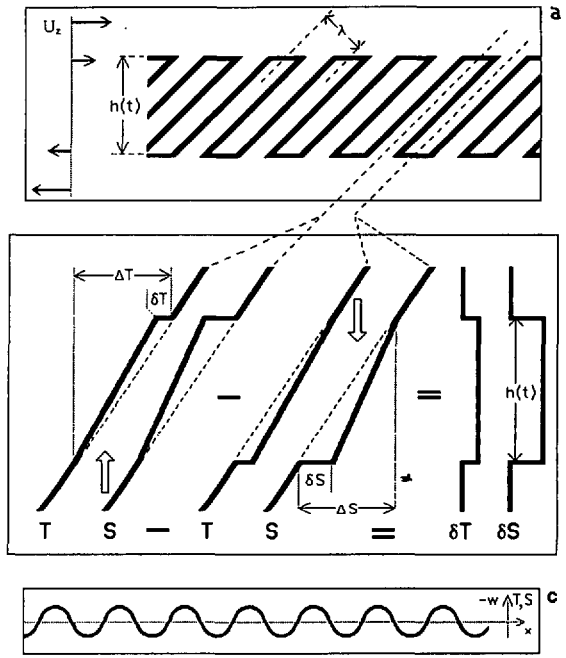


Figure 2. A schematic defining the parameters of the sheared finger model. In the upper panel (a), a vertical cross-section through a zone of tilted fingers is shown. The thick solid lines demark the strong gradients between adjacent fingers and at their intruding tips. The central panel (b) displays temperature and salinity profiles along the dashed lines in (a) for up- and downgoing fingers (left and center) and the contrasts between fingers (right). Temperature and salinity are continuous at the inlet to a finger, vary smoothly over its length and are discontinuous at the intruding tip. Upgoing fingers are lighter than the surrounding fluid, downgoing fingers heavier. Gradients inside the fingers (solid lines) are weaker than in the unperturbed fluid (dashed lines). The finger height $h$ lengthens in time. Sinusoidal structure for finger temperature, salinity and vertical velocity is assumed (c).

uniform background vertical gradients of temperature $\overline{T}_z$, salinity $\overline{S}_z$, and shear $U_z$. The thick lines represent the strong gradients that exist between adjacent fingers and at their intruding tips (Piacsek and Toomre, 1980).

The fingers lengthen in time due to their buoyancy-driven motions, drawing fluid in at their inlets that has been displaced by the adjacent intruding tips. Temperature and salinity are continuous at the inlets, have reduced gradients within the fingers and discontinuities at the intruding tips (Fig. 2b). Because salt has such a low molecular diffusivity, there is little diffusion of salt between fingers, and so the salinity gradient is governed by advection. A column of water is stretched to twice its original height in a finger, so the salinity gradient inside fingers is half that of the background (Fig. 3). Since temperature diffuses more rapidly, the contrasts between adjacent fingers will be

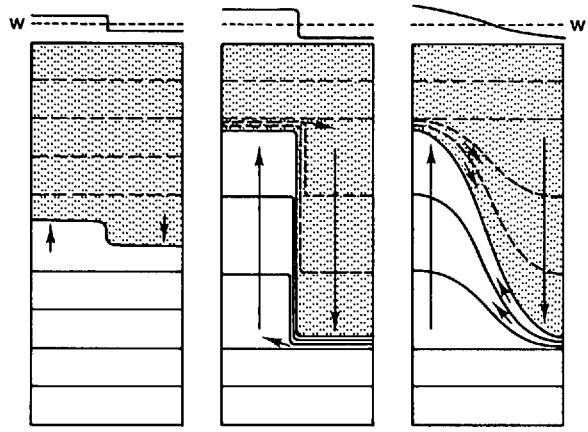


Figure 3. Cartoon illustrating the effect of a growing finite-length finger's velocity $w$ on a property of low diffusivity. The left panel shows initial conditions. The central and right panels correspond to square and sinusoidal $w$-structure, respectively. Water pushed aside by the intruding tip of one finger joins the fluid in the adjoining, oppositely-flowing finger. Conservation of volume then dictates that the vertical gradient in the finger will be half that of the background.

weaker and temperature-gradients in fingers are closer to the background value (Kunze, 1987).

Sinusoidal finger structure is assumed (Fig. 2c), and will be taken to be a square planform $\sin(k_x x)\sin(k_y y)$ in the horizontal (Stern, 1976) where $k_x = 0$ corresponds to salt sheets (Linden, 1974). The vertical structure within the fingering zone will be a superposition of the reduced gradients $T_z$ ($<\overline{T}_z$) and $S_z$ ($<\overline{S}_z$), and sinusoidal finger structure. Mathematical expressions corresponding to the above description are

$$\begin{aligned} T &= T_o + T_z z + \delta T(t) \cdot \sin(k_x x + k_z z)\sin(k_y y) \\ S &= S_o + S_z z + \delta S(t) \cdot \sin(k_x x + k_z z)\sin(k_y y) \end{aligned} \tag{1}$$

where $\delta T(t)$ and $\delta S(t)$ are the contrasts between adjacent fingers relative to the horizontal average, the finger gradients

$$\begin{aligned} T_z &= \overline{T}_z + \frac{2\delta T}{h} \\ S_z &= \overline{S}_z + \frac{2\delta S}{h} \end{aligned} \tag{2}$$

(Fig. 2b) and the finger height

$$h(t) = h_o + \int_0^t 2w \cdot dt. \tag{3}$$

The equations of motion for tilted salt fingers in a uniform shear $U_z$ (with the coordinate system oriented in the direction of the shear) are

$$\begin{aligned}
&\boxed{\frac{\partial u}{\partial t} + \boxed{U\frac{\partial u}{\partial x}} - \nu\nabla^2 u + U_z w = -\frac{\partial p}{\partial x}} \\
&\frac{\partial w}{\partial t} + \boxed{U\frac{\partial w}{\partial x}} - \nu\nabla^2 w = \boxed{-\frac{\partial p}{\partial z}} + g(\alpha\delta T - \beta\delta S) \\
&\frac{\partial \delta T}{\partial t} + \boxed{U\frac{\partial \delta T}{\partial x}} - \kappa_T\nabla^2\delta T + T_z w = 0 \\
&\frac{\partial \delta S}{\partial t} + \boxed{U\frac{\partial \delta S}{\partial x}} - \kappa_S\nabla^2\delta S + S_z w = 0 \\
&\boxed{\frac{\partial u}{\partial x} + \frac{\partial w}{\partial z} = 0}
\end{aligned} \tag{4}$$

The terms in boxes in (4) are those not found in the equations of motion for untilted, unsheared salt fingers (Stern, 1960). These include (i) the $u$-momentum equation, (ii) a pressure term in the $w$-momentum equation, (iii) conservation of mass in its incompressible form and (iv) advection $U\partial/\partial x$ of the fingers by the background flow [in double boxes]. Note that the background properties ($U$, $U_z$, $\overline{T}_z$, $\overline{S}_z$) are not constrained to be steady; WKB theory allows them to change provided they do so on a timescale long compared to that of the fingers. Looking for solutions proportional to $\exp[i(k_x x + k_y y + k_z z)]$, (4) becomes

$$\begin{aligned}
&\frac{Du}{Dt} + \nu k^2 u + U_z w + ik_x p = 0 \\
&\frac{Dw}{Dt} + \nu k^2 w + ik_z p - g(\alpha\delta T - \beta\delta S) = 0 \\
&\frac{D\delta T}{Dt} + \kappa_T k^2 \delta T + T_z w = 0 \\
&\frac{D\delta S}{Dt} + \kappa_S k^2 \delta S + S_z w = 0 \\
&k_x u + k_z w = 0,
\end{aligned} \tag{5}$$

where $D/Dt = \partial/\partial t + ik_x U$. Letting the tilt $k_z/k_x = s$, continuity yields

$$u = -\frac{k_z}{k_x} w = -sw \tag{A6}$$

and the two momentum equations can be coupled together by eliminating their pressure terms to obtain

$$\frac{Dw}{Dt} + s\frac{D(sw)}{Dt} + \nu k^2(1 + s^2)w - sU_z w - g(\alpha\delta T - \beta\delta S) = 0. \tag{7}$$

Stern (1960) showed that even the maximum $D/Dt$ ($\equiv$ growth rate $\sigma_o$) is much less than $\nu k^2$ (see also Fig. 2 of Kunze, 1987). Therefore, the time-derivatives can be neglected in (7). The problem then reduces to a diagnostic for $w$ and two evolution equations for $\delta T$ and $\delta S$

$$\begin{aligned} w &= \frac{g(\alpha\delta T - \beta\delta S)}{\nu k^2(1 + s^2) - sU_z} \\ \frac{D\delta T}{Dt} &= -\kappa_T k^2 \delta T - T_z w \\ \frac{D\delta S}{Dt} &= -\kappa_S k^2 \delta S - S_z w. \end{aligned} \tag{8}$$

In a shear field, the finger wavevector will be continuously-deformed just as is the wavevector of internal waves in vertical shear (Lighthill, 1978; Phillips, 1966). From WKB theory (e.g., Frankignoul, 1970; Olbers, 1981), the horizontal wavevector is invariant in a vertical shear but the vertical wavenumber changes continuously

$$\boxed{\frac{dk_z}{dt} = -k_x U_z} \tag{9}$$

which implies that the tilt $s$ varies with time

$$s = \frac{k_z}{k_x} = s_o - \int_0^t U_z \cdot dt, \tag{10}$$

where $s_o$ is the initial tilt. The total wavenumber will behave parameterically as

$$k^2 = k_x^2(1 + s^2) + k_y^2 \tag{11}$$

where $k_x^2 + k_y^2 = k_H^2$ is the square horizontal wavenumber. Eq. (9) is the same mechanism that pushes shear and buoyancy microstructure toward high wavenumber and molecular dissipation in classical turbulence theory (Batchelor, 1959).

## 3. A Numerical model

Since the wavevector changes continuously, it is not possible to find an analytic similarity solution to (8) valid for all time. The dependence of the *initial* growth rate on wavenumber and tilt is presented in Appendix B. In this section, the evolution of fingers in shear is computed numerically. Eqs. (8)–(9) were solved with a Runge-Kutta

Table 1. Parameter values used for the figures. Values are typical of the thermohaline staircase east of Barbados (Mazeika, 1974; Boyd and Perkins, 1987; Schmitt *et al.*, 1987; Gregg and Sanford, 1987).

| Variable | Value |
|---|---|
| $\nu$ | $10^{-6}$ m$^2$/s |
| $\kappa_T$ | $1.4 \times 10^{-7}$ m$^2$/s |
| $\kappa_S$ | $1.1 \times 10^{-9}$ m$^2$/s |
| $g$ | 9.8 m/s$^2$ |
| $\alpha$ | $2 \times 10^{-4}$ °C$^{-1}$ |
| $\beta$ | $7.5 \times 10^{-4}$‰$^{-1}$ |
| $L_o$ | 20 m |
| $l_i$ | 2 m |
| $\overline{T}_z$ | 0.3 °C/m |
| $\overline{S}_z$ | 0.05 ‰/m |
| $N$ | $1.5 \times 10^{-2}$/s |
| $P_N = 2\pi/N$ | 7 min |
| $R\rho$ | 1.6 |
| $\lambda_{Hfg}$ | 3.1 cm |
| $U_z$ | $6.3 \times 10^{-3}$/s |
| $f$ | $3.5 \times 10^{-5}$/s |
| $P_f = 2\pi/f$ | 2 days |
| $Ri$ | 6 |

routine (Press *et al.*, 1986) using a time-step of $2\pi/(200N)$. Environmental parameters were set to values typical of the interfaces in the thermohaline staircase east of Barbados (Table 1). Specifically, salinity gradient $\overline{S}_z = 0.05$‰/m, density ratio $R\rho = 1.6$ and vertical shear $U_z = 6.3 \times 10^{-3}$/s ($Ri = 6$). This ignores the interface substructure described by Marmorino (1989) which could result in larger fluxes and microstructure.

Horizontal structure corresponding to a checkerboard pattern ($k_x = k_y$) (Fig. 4a) and sheet form ($k_x = 0$) (Fig. 4b) will be considered. The fingers are seeded with initial heights $h_o = 2w_o/\sigma_o = \pi/(2k_H)$, where $k_H$ is the horizontal wavenumber (11) and $\sigma_o$ the growth rate (B1) at $t = 0$. This initial condition is consistent with (3) and an isotropic initial structure that might be caused by turbulence (Kunze, 1987). The initial temperature and salinity anomalies are then set with (8) assuming that $D/Dt = \sigma_o$ (B1). As will be shown (see Fig. 12), the results are insensitive to initial conditions.

*a. In steady shear.* Linden's (1974) laboratory experiments demonstrated that the dominant double-diffusive instability in *steady* shear is vertical sheets aligned with the shear ($k_x = 0$). He argued that instabilities with nonzero wavenumbers in the direction of the shear were stabilized by the shear. Figure 5 suggests an alternative

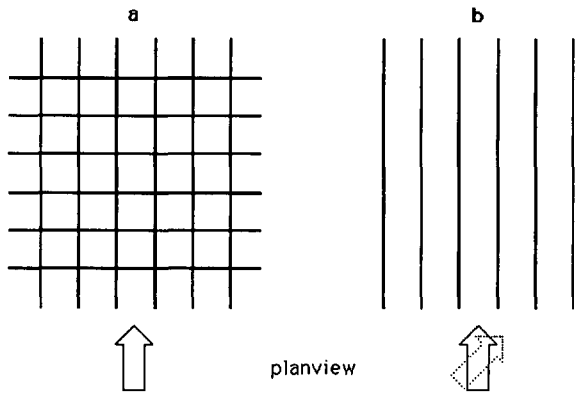


Figure 4. Plan view of fingers with (a) a square planform ($k_x = k_y = k_H/\sqrt{2}$) and (b) a sheet form ($k_y = 0$) initially aligned with the shear. Inertial shear turns clockwise with time as indicated by the dotted arrow.

explanation. Plotted are the time-evolutions of the normalized finger height $h/h_o$ and vertical velocity $w/w_o$, where $h_o$ and $w_o$ are initial values, for horizontal wavelengths of 2–7 cm and $k_x = k_y$ (Fig. 4a). The fingers do not grow. They are tilted over so rapidly that the vertical velocity diminishes monotonically. The finger height does not change significantly. Therefore, *unless* fingers form sheets aligned with the shear ($k_x = 0$; Fig. 4b), they are tilted over and molecularly damped too rapidly to contribute significant fluxes.

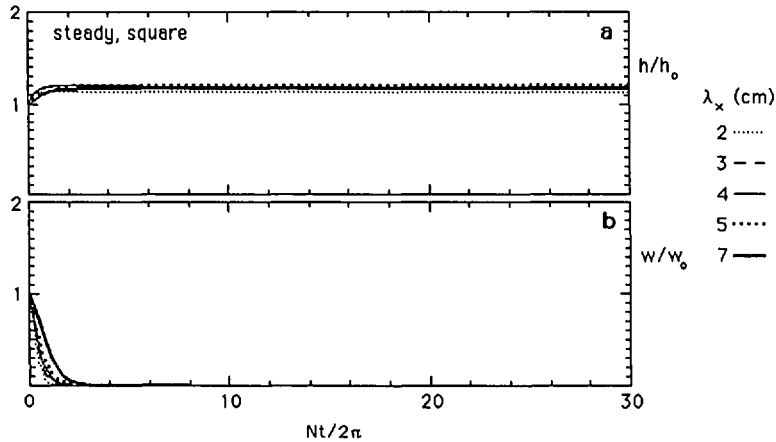


Figure 5. The time evolution of normalized (by their initial values) finger height $h/h_o$ (upper panel) and vertical velocity $w/w_o$ (lower panel) for square planform fingers with horizontal wavelengths ranging from 2–7 cm in a shear of $Ri = 6$. The vertical velocity decays without growing. As a consequence, the finger height does not increase significantly.

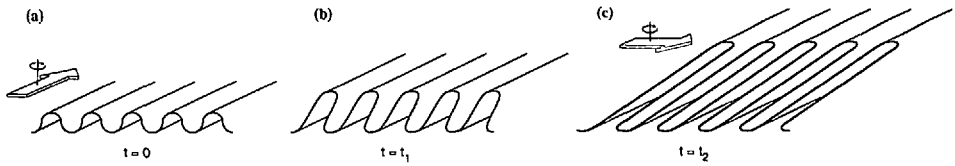


Figure 6. Schematic illustrating the evolution of salt sheets in near-inertial shear. At their inception $t = 0$ (a), the sheets are assumed to be aligned with the shear. As time progresses, the shear turns clockwise with an inertial period. This introduces a component of the shear normal to the sheet crests which will tilt them over as they grow (b, c).

On the other hand, in steady shear sheet growth is the same as unsheared square-planform fingers because the equations of motion (4) reduce to the unsheared form when $\partial/\partial x = ik_x = 0$.

*b. In inertially-rotating shear.* However, in the deep ocean, shear is not steady but near-inertial (Sanford, 1975; D'Asaro, 1984, 1985; Kunze *et al.*, 1990). In particular, the shear during C-SALT had periods consistent with near-inertial (~48 h at 12N) (see Fig. 2 of Gregg and Sanford, 1987). The shear for these waves has no node but rotates in both depth and time. This, along with the ubiquity of near-inertial wave motion in the ocean (Fu, 1981), implies that there should always be shear at any location as is observed (Eriksen, 1978; Kunze *et al.*, 1990).

It will be assumed that the fingers start growing as sheets aligned with the shear $(k_x, k_y) = (k_H, 0)$ (Fig. 4b; Fig. 6a) where the shear is in the $y$-direction at $t = 0$. This allows us to continue to use (4) even though it does not include a $v$-momentum equation. As time progresses, the shear rotates, $(U_z, V_z) = |\mathbf{V}_z|\,(\sin(ft), \cos(ft))$, introducing a slowly-growing component normal to the sheets (Fig. 6b, c).

Kunze (1987) found that unsheared fingers grew for about ten buoyancy periods (~1 h; Table 1) before reaching a critical Stern (1969) or inverse finger Richardson number of four. In ten buoyancy periods, a near-inertial shear of magnitude $0.4N$ that is initially aligned with sheets will turn enough to produce an across-sheet shear of $0.05N$ ($Ri = 400$). This is sufficient to cause tilting $\sim O(20°)$ in ten buoyancy periods. Therefore, it is possible that (i) sheets could grow significantly before being tilted and damped, yet (ii) be significantly tilted before becoming unstable. The first point is borne out by Figure 7 which displays the time-evolution of the normalized (by their initial values) finger height $h/h_o$ and vertical velocity $w/w_o$ for horizontal wavelengths of 2–7 cm. Fingers with 3–4 cm horizontal wavelengths (fastest-growing) achieve almost 100 times their initial height before their wavelength becomes sufficiently small that molecular processes prevent further growth. This occurs at a wavelength of ~1 cm.

To demonstrate that shear-tilting can reproduce the observed temperature and optical (salt?) microstructure, Figure 8 displays the normalized vertical finger gradients of temperature and salinity, $\delta T_z/|\nabla_o T_o|$ and $\delta S_z/|\nabla_o S_o|$ as functions of vertical wavelength. Recall that the vertical wavenumber increases in magnitude in time (9).

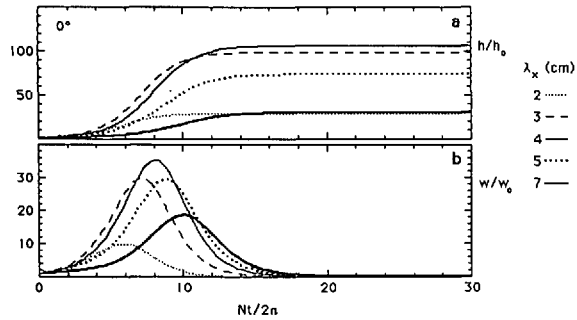


Figure 7. The time-evolution of salt sheets with wavelengths ranging from 2–7 cm in inertially-rotating shear of $Ri = 6$. The normalized finger height $h/h_o$ is shown in the upper panel and vertical velocity $w/w_o$ in the lower panel. The sheets are initially aligned with the shear (Fig. 6a). They tilt over and are damped more slowly than square planform fingers (Fig. 5) which feel the full effect of shear. The vertical velocities grow for ~7 buoyancy periods, attaining magnitudes up to 35 times their initial value before decaying. The finger heights reach up to 100 times their initial value for horizontal wavelengths similar to the unsheared fastest-growing wavelength of 3 cm.

Thus, the vertical wavelength diminishes in time and time increases to the left in Figure 8. As t he sheets grow, the temperature- and salinity-gradients increase until the scale becomes small enough that molecular diffusion smooths out their structure. This occurs at a wavelength of 3 cm for temperature and 1 cm for salt. The salt wavelength is identical to that of the optical striations in the shadowgraph images from the fingering-favorable parts of the profiles (Fig. 1b), supporting the hypothesis that the observed laminae are due to salt. The temperature scale is larger than the salt scale, though not as large as the 6-cm temperature vertical wavelength reported by Gregg

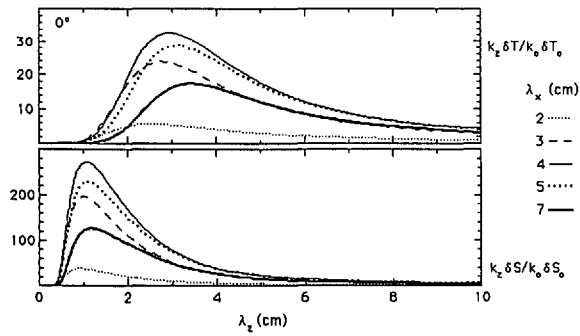


Figure 8. Normalized (by the initial gradients) vertical temperature- (upper panel) and salinity-gradient (lower panel) vs. vertical wavelength for horizontal wavelengths of 2–7 cm. The vertical wavelength decreases in time (9), so time increases to the left. As fingers grow, their vertical gradients increase until their wavelength becomes sufficiently small that molecular diffusion eradicates the signature. This occurs at a vertical wavelength of 3 cm for temperature and 1 cm for salt.

and Sanford (1987). As discussed in the next section, this may be the vertical scale at which the sheets go unstable.

## 4. Fluxes

Replicating the scales of the observed temperature and salinity microstructure does not guarantee that the model is correct. If appropriate, the model should also be able to reproduce the observed dissipation rates ($\epsilon \sim 5 - 10 \times 10^{-10}$ W/kg in the interfaces and $\sim 1.4 - 3 \times 10^{-10}$ W/kg in the layers; Gregg and Sanford, 1987; Fleury and Lueck, 1990) and Cox numbers (~10; Marmorino *et al.*, 1987; Fleury and Lueck, 1990; Gregg and Sanford, 1987). In this section, the model is used to try to simulate the C-SALT microstructure variances.

In a buoyancy-driven mixing layer, the dissipation rate must be less than or equal to the forcing buoyancy-flux, $\epsilon \leq F_b$. Convection theory (Businger *et al.*, 1971) suggests that $\epsilon \simeq F_b$ and this has been observationally verified in the atmosphere (Caughey and Palmer, 1979) and ocean (Shay and Gregg, 1986). Therefore, the buoyancy-flux will be assumed equal to the layer dissipation rate.

Fluxes are determined by combining molecular diffusion, $g\kappa_T\alpha\overline{T}_z$ and $g\kappa_s\beta\overline{S}_z$, with average salt-finger fluxes, $g\alpha\langle w\delta T\rangle$ and $g\beta\langle w\delta S\rangle$, from the model where $\langle\cdot\rangle = (1/t_c)\cdot\int_0^{t_c}(\cdot)\,dt$. The *critical time* $t_c$ is set by some amplitude constraint on finger growth. In Section 4a, it corresponds to the maximum instantaneous buoyancy-flux. In Section 4b, it is the time when the instantaneous inverse finger Richardson number $(\nabla \times V)^2/N^2$ exceeds a specified critical value. Molecular diffusion is included because it is always present; it will not affect the interface dissipation rates or Cox numbers. Internal wave-generated turbulence appears to be too weak to contribute significant interfacial fluxes (Gregg, 1989) though it will contribute to the Cox number and dissipation variance; this view differs from that of Marmorino (1990) and Fleury and Lueck (1990) who argue that turbulence contributes enough flux to raise the flux ratio by a factor of ~1.1. Isopycnal mixing cannot be evaluated but would not produce the staircase structure. As discussed by McDougall (1990) (see Appendix A), interface migration will contribute little to the fluxes though it becomes crucial when considering water-mass (layer property) changes.

*a. Unconstrained fluxes.* First we investigate the case where sheet growth is unrestricted except by tilting. These results will be referred to as *unconstrained* since no external constraint is placed on the finger amplitude. Figure 9 shows the average flux ratio $R_F = \alpha\langle F_T\rangle/\beta\langle F_S\rangle$, dissipation rate $\langle\epsilon\rangle$, buoyancy-flux $\langle F_b\rangle$, Cox number $\langle C_T\rangle$, and inverse finger Richardson number $Ri_f^{-1}$ contoured against horizontal wavelength $\lambda_x$ and *initial* tilt angle $\theta_o$. The averaging assumes that when the sheets start to decay (at about 14 buoyancy periods in Fig. 7), new sheets begin to form.

The peak average model dissipation rates and buoyancy-fluxes (Fig. 9) are two orders of magnitude larger than the C-SALT microstructure values. Therefore, some

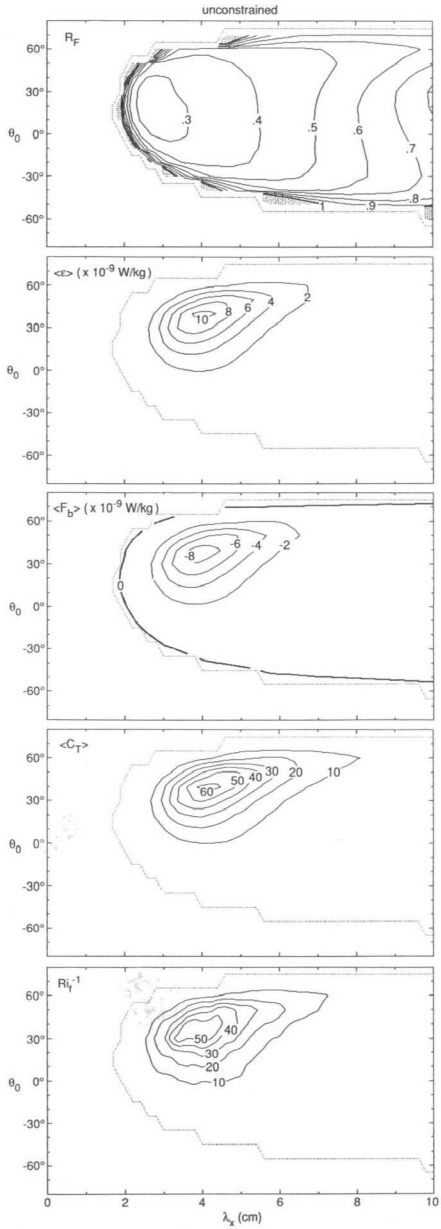


Figure 9. The *average* flux ratio $R_F = \alpha\langle F_T\rangle/\beta\langle F_S\rangle$, dissipation rate $\langle\epsilon\rangle$, buoyancy-flux $\langle F_b\rangle$, Cox number $\langle C_T\rangle$, and inverse finger Richardson number $Ri_f^{-1}$ contoured against horizontal wavelength $\lambda_x$ and initial tilt angle $\theta_o$ for unconstrained fingers. The peak buoyancy-fluxes of $-80 \times 10^{-10}$ W/kg and dissipations of $100 \times 10^{-10}$ W/kg are two orders of magnitude larger than the C-SALT observations.

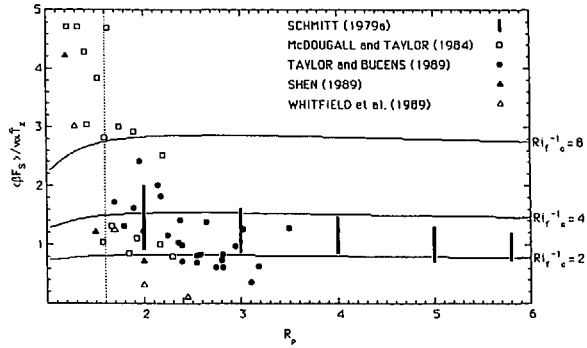


Figure 10. The *average approximate* Stern number $\beta\langle F_S\rangle/(\nu\alpha\overline{T}_z)$ vs. density ratio $R_\rho$ from laboratory measurements and numerical simulations. The solid curves are from the Kunze (1987) model for various *critical* $Ri_f^{-1}$ (numbers along the right axis). For $R_\rho = 1.6$ (dotted vertical line), the data range from critical $Ri_f^{-1} = 3$–16. Taylor and Bucens (1990) suggest that the very high values at low $R_\rho$ found by McDougall and Taylor (1984) may be due to their unique initial conditions. However, similar values are found in numerical simulations (Shen, 1989; Whitfield *et al.*, 1989).

constraint must limit the growth of sheets. For an untilted finger model, Kunze (1987) found that halting finger growth when a Stern or inverse finger Richardson number exceeds four approximately reproduces the observed C-SALT microstructure.

*b. Constrained fluxes.* What controls the magnitude of salt-fingering fluxes has been a longstanding question in the field and is still unresolved. Stern (1969) proposed that fingers grow until their normalized buoyancy-flux, $F_b/\nu N^2$ (henceforth referred to as the Stern number), exceeds a critical value $\sim O(1)$ and then are disrupted by 'large-scale' (collective) instability of the fingers. Holyer (1981) showed that the critical Stern number should be $1/3$, however, in a later paper (1984) identified a high-wavenumber intrusive instability which arose at Stern numbers $\sim O(10^{-2})$.

For vertical fingers, the Stern number is identical to an inverse *finger* Richardson number, $Ri_f^{-1} = (\nabla \times V)^2/N^2 = (\nabla_H w)^2/N^2$, where the horizontally-sheared vertical velocity has replaced the vertically-sheared horizontal velocity of the conventional Richardson number (Kunze, 1987). Figure 10 displays laboratory (Schmitt, 1979a; McDougall and Taylor, 1984; Taylor and Bucens, 1989) and numerical (Shen, 1989; Whitfield *et al.*, 1989) estimates of the *average approximate* Stern number $\beta\langle F_S\rangle/(\nu\alpha\overline{T}_z)$ as a function of density ratio $R_\rho$ along with model curves of this quantity (Kunze, 1987) for *critical* $Ri_f^{-1} = 2$, 4 and 8 (assuming fastest-growing fingers). Neither the lab nor numerical results support fingers being disrupted at Stern numbers $\sim O(10^{-2})$ even though Whitfield *et al.* (1989) reported that perturbations on fingers grew at rates consistent with Holyer's (1984) theory. The numerical values (Shen 1989; Whitfield *et al.*, 1989) might be questioned because their Prandtl and Lewis numbers are much closer to one than appropriate for heat-salt fingers, but this is more

likely to affect values at high $R_\rho$. Taylor and Bucens (1989) suggest that the very high values found for $R_\rho < 2$ by McDougall and Taylor (1984) may be due to their unique initial conditions. However, the fact that numerical simulations independently suggest the same $R_\rho$-dependence for the Stern number raises doubts about the universality of a constant Stern number constraint. For the C-SALT density ratio $R_\rho = 1.6$, $\langle \beta F_S \rangle / (\nu \alpha \overline{T}_z)$ is scattered between 1–5, which corresponds to critical $Ri_f^{-1}$ between 3–16 (curves in Fig. 10).

Kunze (1987) showed that for the 2-m thick interfaces in the staircase east of Barbados, a critical inverse finger Richardson number of four implied fluxes roughly compatible with the measured buoyancy-fluxes (Gregg and Sanford, 1987) but two orders of magnitude smaller than predicted by the laboratory $\Delta S^{4/3}$ law (Turner, 1967; Kelley, 1990. This constraint also gives results consistent with heat-fluxes inferred off the California coast (Osborn, 1988) and the salt budget of a Mediterranean lens (Hebert, 1988). To produce fluxes consistent with the $\Delta S^{4/3}$ flux law, interfaces can be no more than ~30-cm thick.

For tilted fingers, the inverse finger Richardson and Stern numbers are not identical, but related through

$$Ri_f^{-1} = \frac{(\nabla \times V)^2}{N^2} = \frac{(\nabla_H w)^2 (1 + s^2)^2}{N^2} = \frac{F_b}{\nu N^2}(1 + s^2)^2 \tag{12}$$

where both the vertical velocity $w$ and tilt $s$ vary in time. Because these two hypothesized constraints differ, both Stern and inverse finger Richardson number constraints were applied to growing sheets. However, the results did not differ significantly, so only the $Ri_f^{-1}$ constraint results are presented here. It will be presumed that the fluxes are disrupted when $Ri_f^{-1}$ exceeds a critical value and that new sheets immediately begin to grow. Therefore, averaging is carried out from $t = 0$ to the time $t_c$ when the critical inverse finger Richardson number is exceeded. This is a gross simplification. Undoubtedly, a fingering field is made up of an ensemble of fingers at various stages of growth and instability disrupts the finger fluxes in a complicated interactive way. However, this scheme does at least include fingers at all stages of growth in the average.

The first sheets to go critical for $Ri_f^{-1} c = 4$ do so in 5.5 buoyancy periods ($Nt_c/2\pi = 5.5$, lowermost panel in Fig. 11). They correspond initially to fastest-growing vertical fingers ($\lambda = \lambda_x \sim 3$ cm, $\theta_o \sim 0°$). Vertical fingers grow most rapidly because a buoyancy anomaly drives weaker (by $s^{-1}$) along-sheet flows along tilted trajectories and even weaker (by $s^{-2}$) vertical motions. Though vertical sheets become tilted in time, more rapid initial growth appears to be the most crucial factor. These 'first-to-go-unstable' sheets have a flux ratio $R_F = 0.85$ (stippled patch in uppermost panel of Fig. 11), identical to the C-SALT layer density ratio, but their average dissipations, buoyancy-fluxes and Cox numbers are smaller than the C-SALT observations. Choosing a larger critical inverse finger Richardson number will better repro-

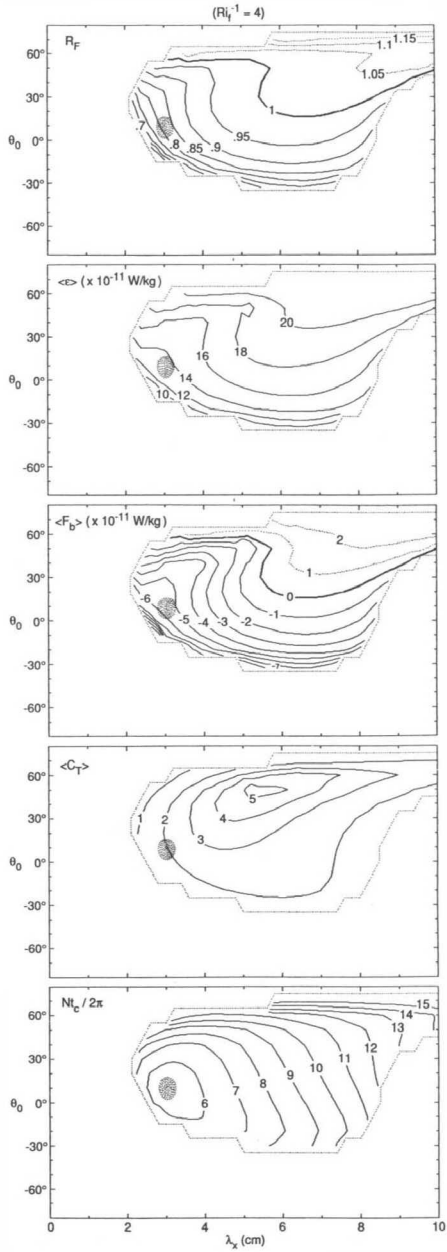


Figure 11. The *average* flux ratio $R_f$, dissipation rate $\langle\epsilon\rangle$, buoyancy-flux $\langle F_b\rangle$ and Cox number $\langle C_T\rangle$ for a critical inverse finger Richardson number of four contoured against horizontal wavelength and *initial* tilt angle. Also contoured is the time $Nt_c/2\pi$ it takes the sheets to reach critical value. Only sheets inside the contoured region attain $Ri_f^{-1}c = 4$. The first sheets to go critical (at $Nt_c/2\pi = 5.5$, lowermost panel) are stippled in all panels. They will disrupt the other fingers' growth and dominate the fluxes. Their wavelengths and initial tilts correspond to fastest-growing fingers ($\lambda_x = 3$ cm, $\theta_o = 0°$). Their flux ratios are ~0.8–0.85, dissipation rates ~$13 \times 10^{-11}$ W/kg, buoyancy-fluxes ~5–$6 \times 10^{-11}$ W/kg and Cox numbers 2. The ridge of high dissipation rate $\langle\epsilon\rangle$ and buoyancy-flux $\langle F_b\rangle$ running from $\lambda_x = 3$ cm, $\theta_o = 0°$ to ~8 cm, 60° corresponds to sheets which initially have *total* wavelengths near the fastest-growing wavelength. Thus, sheets with the fastest-growing wavelength grow more than sheets of the same tilt with either higher or lower wavenumber.

duce the C-SALT dissipation rate, buoyancy-flux and Cox number, as well as be more consistent with the high critical values in Figure 10, but then the flux ratio will be smaller than the layer density ratio. This is not a concern if we believe McDougall's (1990) arguments (see Appendix A) that the layer density ratio does not constrain the flux ratio so the C-SALT finger flux ratio is unknown.

The sheets go unstable at tilt angles of 15–40°, depending on seed amplitudes. But if they go unstable before being fully tilted over, how is the optical microstructure produced? This is easily addressed. Instability of the sheets will disrupt fluxes and lead to smoothing of both velocity and temperature microstructure because of the higher molecular diffusivities associated with these quantities. But passive salinity microstructure will remain on scales too small to drive vertical motions. It will continue to be tilted by the persistent shear until it reaches the 1-cm wavelength where molecular diffusion can eradicate it (Fig. 8). In this spirit, Figure 12 displays vertical slices of the salinity and temperature microstructure as might be seen with a shadowgraph (neglecting parasitic instabilities). The temperature and salinity microstructure have the same horizontal wavelength but different vertical wavelengths because of the greater degree of tilt for salt. The temperature contribution to the optical signal will be much weaker than the salt because of its larger wavelengths and therefore weaker Laplacian.

Following common practice in turbulence measurements, the C-SALT microstructure investigators assumed isotropy and multiplied their measured shear variances by $1\frac{1}{2}$ to obtain dissipation rates and their temperature-gradient variances by 3 to obtain Cox numbers. For the model described here, these factors will not be correct because the sheets are not fully isotropic. The relationships between the 'isotropized' and true values for the tilted sheet model are

$$\begin{aligned} \text{tow } C_T &= \frac{3}{(1.5)^2(1+s^2)} C_T \\ \text{tow } \epsilon &= \frac{15}{2(1.5)^2(1+s^2)^2} \epsilon, \end{aligned} \tag{13a}$$

where the factor of $(1.5)^2$ arises because tows are not always normal to the sheet crests so underestimate the horizontal gradients. Likewise,

$$\begin{aligned} \text{profile } C_T &= \frac{3}{(1+s^{-2})} C_T \\ \text{profile } \epsilon &= \frac{15}{2(1.5)^2(1+s^{-2})} \epsilon \end{aligned} \tag{13b}$$

depend on tilt $s$.

The sensitivity of the average model dissipation rates (true and 'isotropized'), Cox numbers (true and 'isotropized'), buoyancy-flux and flux ratio to initial magnitudes $h_o^2$ [normalized by $\pi^2/(4k_o^2)$] and critical $Ri_f^{-1}$ is examined in Figure 13 assuming that

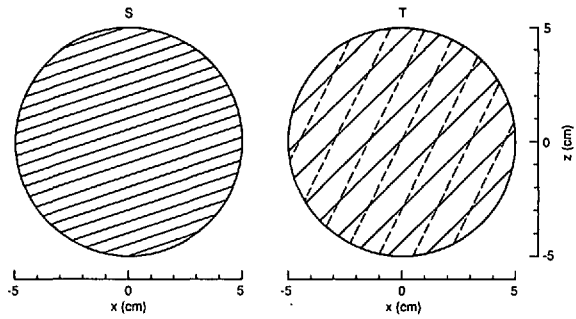


Figure 12. Vertical cross-sections of the dominant sheet salinity and temperature microstructure assuming that, when the sheets 'break' at a critical $Ri_f^{-1} = 3$–16 [$\theta_f = 15°$ (dashed) to 40° (solid)], the sheet temperature microstructure is disrupted and smoothed by molecular processes, while the salt structure continues to be tilted.

when fastest-growing sheets go unstable, they disrupt the fluxes associated with other sheets and so dominate the overall fluxes (this is true for the fluxes but may underestimate the Cox numbers by as much as a factor of two). Except for profile dissipation rate, there is little sensitivity to the initial conditions provided that the seed height is large enough that the sheets can become critical (right of dotted line). This insensitivity is a consequence of nearly exponential growth.

On the other hand, there is strong dependence on the critical inverse finger Richardson number. Values inferred from the C-SALT microstructure measurements are stippled. The domain constrained by the buoyancy-flux (layer dissipation rate) is stippled in all the panels. The buoyancy-flux implies smaller dissipation rates and Cox numbers than those observed. One explanation for this discrepancy is that there is large uncertainty in the measurements. Intercomparisons on the equator indicate factors of 2–3 uncertainty between different instruments and computational methods (Gregg, personal communication, 1990). However, in C-SALT the discrepancy appears in measurements from the same sensors (e.g., layer and interface dissipation rate). Gregg and Sanford (1987) also caution that temperature microstructure may bias the interface dissipation rates high but this would not explain the excess Cox number. Another explanation may be that the model does not explicitly include variance due to the instabilities that disrupt the sheets. These parasitic perturbations will enhance the interface microstructure (dissipation rate and Cox number) relative to the buoyancy-flux, making these fields more jumbled and chaotic as found in numerical simulations (Shen, 1989; Whitfield *et al.*, 1989).

## 5. Summary

A model for the interaction of salt fingers with oceanic shear has been described. This work extends earlier vertical finger models (Stern, 1960; Linden, 1974; Schmitt, 1979b; Kunze, 1987) by allowing fingers to be tilted by shear and considering unsteady

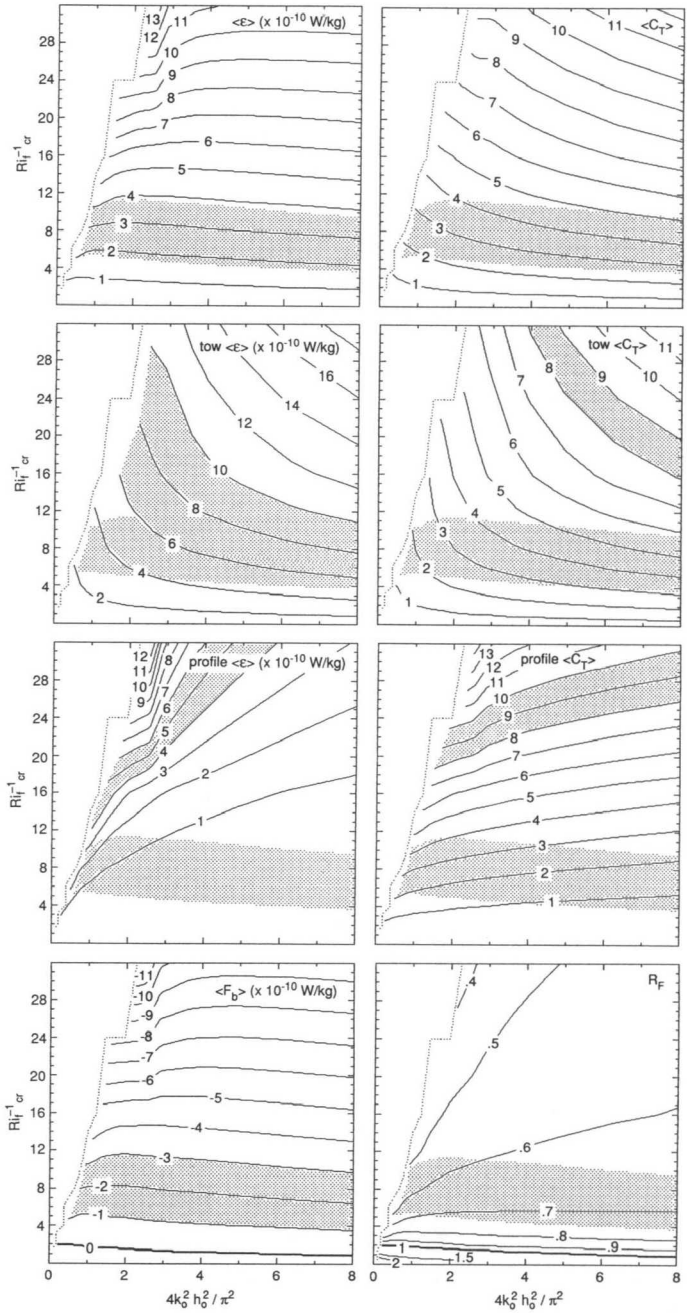


Figure 13. Contours of average Cox number $\langle C_T \rangle$, dissipation rate $\langle \epsilon \rangle$ [model, 'isotropized' tow and 'isotropized' profile], buoyancy-flux $\langle F_b \rangle$ and flux ratio $R_F$ for the first sheets to go critical ($\lambda_x = 3$ cm, $\theta_o = 0°$) as a function of critical inverse finger Richardson number $Ri_f^{-1}c$ and initial conditions $h_o^2/(\lambda_o/4)^2$. Stippling demarks the range of values from the C-SALT observations. The domain defined by the C-SALT buoyancy-fluxes (≡layer dissipation rate) is stippled in all the panels as well.

shear. Analytic solutions are no longer possible and the equations (8)–(9) must be integrated numerically in time. Even for the relatively weak shear found in the thermohaline staircase east of Barbados ($Ri = 6$), square planform ($k_x = k_y$) fingers are tilted over so rapidly that they are damped out by molecular processes before they can produce significant fluxes. This is consistent with the laboratory and analytic work of Linden (1974) which demonstrated that, in a steady shear $U_z$, the only instability that can grow is in the form of sheets aligned with the shear ($k_x = 0$).

In the C-SALT staircase as elsewhere in the ocean, shear is not steady but near-inertial, turning to produce an across-sheet component of shear even for initially aligned sheets. This occurs slowly enough that sheets have a chance to grow before being significantly tilted. The model produces tilted sheets with temperature and salinity microstructure consistent with the C-SALT measurements. In particular, the 1-cm limiting wavelength for salt is identical to that of the nearly-horizontal laminae in the optical shadowgraph images (Fig. 1; Kunze *et al.*, 1987).

In light of these results and the prevalence of near-inertial shear in the ocean, it is difficult to explain how vertical banding has been observed elsewhere (Williams, 1975, 1981; Schmitt and Georgi, 1982). Internal wave shear was weaker ($\sim 0.4N$) in, above and below the thermohaline staircase east of Barbados than the $0.7-1.0N$ typically found in the pycnocline (Garrett and Munk, 1979; Evans, 1981). Even a few kilometers outside the staircase, shears were more typical (Gregg, personal communication, 1990). It may be that in the lower density ratios found below the Mediterranean salt tongue and in the Tyrrhenian Sea (Williams, 1975), shear is weak enough that fingers can grow without being significantly tilted. This would require shears less than $0.1N$.

Allowing the model sheets to grow unbounded except by shear-tilting leads to average microstructure variances two orders of magnitude larger than found by C-SALT microstructure investigators. Halting growth when the Stern (1969) or inverse finger Richardson number exceeds ~4 produces model fluxes of the right order of magnitude. This constraint is also consistent with laboratory and numerical fluxes though these contain considerable scatter at the low density ratios of oceanic interest (Fig. 10). Sheets with horizontal wavelengths of ~3 cm and zero initial tilt, $\theta_o = 0$, (fastest-growing) are the first to go unstable. This is consistent with the ~5–6 cm horizontal wavelengths observed with towed thermistors and conductivity sensors (Marmorino *et al.*, 1987; Lueck, 1987) when account is taken that towed sensors cross sheets at random orientations which leads to an overestimate bias of ~1.5. The nearly-horizontal 1-cm laminae observed with the shadowgraph appear to be salt remnants that have continued to be shear-tilted long after perturbations have disrupted the finger fluxes and temperature/velocity microstructure has been smoothed away by molecular processes. While any mechanism that produces salt microstructure about once an hour would lead to the nearly-horizontal optical laminae in the observed shear, the strong correlation between the banding and fingering-favorable conditions strongly suggests that the salt-fingering form of double diffusion is responsible.

## 6. Discussion

*a. Model limitations.* Stern (1969) and Kunze (1987) have suggested that finger growth is limited by $F_b/(\nu N^2) \sim O(1)$ or equivalently $Ri_f^{-1} = (\nabla \times V)^2/N^2 \sim O(1)$. This poorly understood constraint on finger growth is the weakest link in the model. A constant critical Stern or finger Richardson number cannot explain the dependence on density ratio seen in the laboratory and numerical simulations (Fig. 10). Furthermore, laboratory measurements (Schmitt, 1979a; McDougall and Taylor, 1984; Taylor and Bucens, 1989) and numerical simulations (Shen, 1989; Whitfield *et al.*, 1989) contain considerable scatter at the low density ratios prevalent in the ocean. Taylor and Bucens suggest that fluxes may be sensitive to initial background conditions and these are very different in the lab and ocean. More careful laboratory studies in the $R_\rho = 1$–2 regime and a better dynamical understanding of what disrupts salt-finger fluxes are needed. We are past the point where simple dimensional or stability arguments can provide new insights. Until these issues are resolved, the vertical finger model of Kunze (1987) remains a more straightforward means of estimating fingering fluxes in high-resolution CTD data (e.g., Hebert, 1988).

No single critical value of $Ri_f^{-1}$ can simultaneously reproduce the C-SALT layer dissipation rate (buoyancy-flux), interface dissipation rate and Cox number (with the latter two quantities tending to be too low in the model). This is probably because the model fails to include variance arising from the parasitic instabilities that grow on and ultimately disrupt fingers. Evidence that these instabilities contribute can be seen in the numerical simulations of Shen (1989) and Whitfield *et al.* (1989). Exploring their dynamics is outside the scope of this paper but is clearly essential for (i) understanding the disruption of finger fluxes and (ii) quantifying ocean fluxes given measured microstructure quantities. This limitation implies that salt-finger models cannot yet be used to diagnose fluxes from microstructure measurements of dissipation rate and Cox number. Therefore, the nondimensionalized ratio of these quantities, $\Gamma = \kappa_T N^2 \langle C_T \rangle / \langle \epsilon \rangle$, proposed by Oakey (1988) as a diagnostic for the relative contributions to microstructure from turbulence and salt-fingers can only be thought of as qualitative. This ratio is a measure of mixing efficiency ($\leq 0.2$ for turbulence). Oakey found it significantly greater than one in regions favorable to double diffusion. The model described here finds values of $\Gamma_i = 0.4$ (excluding a contribution from parasitic instabilities) independent of critical $Ri_f^{-1}$ for a Cox number based on interface gradients and ~10 based on smoothed gradients, $\Gamma = \Gamma_i(L_o + l_i/l_i)^2$. Ocean $\Gamma$ depend sensitively on both the finestructure and the parasitic microstructure, neither of which are described by the model. As a possibly related aside, Fleury and Leuck (1990) found that the Cox number depended linearly on the interface thickness unlike this model. This variation may be related to changes in shear with interface thickness which were not measured or reflect a contribution from parasitic perturbations. Alternatively, double diffusion may be affected by internal wave straining $\partial\zeta/\partial z$ of the interface in ways not considered here.

*b. Other implications.* Fingers are thought to go unstable due to perturbations with $k_z \neq 0$. Stern (1969) initially conceived finger instability as collective with groups of fingers losing their energy to motions of large vertical wavelength. Holyer (1981) quantified the Stern number for large wavelength perturbations, obtaining a value of 1/3. But in a later paper (1984) she argued on the basis of Floquet theory that interfinger intrusions with vertical wavelengths comparable to the fastest-growing wavelength would grow at Stern numbers $\sim O(10^{-2})$. Structure with consistent growth rates is observed in numerical simulations (Whitfield *et al.*, 1989), but apparently not affecting the fluxes since the average deduced Stern numbers (Fig. 10) are greater than $10^{-2}$. This may be explicable in terms of the same physics considered here. A simple stability analysis like Floquet theory is *not* appropriate in a field containing shear. Generalizing the shear interaction described in this paper, a high-wavenumber perturbation between fingers will experience finger-induced shear, $\nabla_H w \sim O(N)$, and be rapidly forced to high horizontal wavenumbers, $k_H = -k_z/\nabla_H w \cdot dt$, where it will be eliminated by molecular diffusion. This tilting can be seen in the Hele-Shaw experiments of Taylor and Veronis (1986). It is possible that the high-wavenumber intrusive instability of Holyer (1984) is damped out before it can inhibit the salt-finger fluxes. Instabilities of larger wavelength can grow relatively unaffected by the shear to ultimately disrupt the fingers.

Unexplained is why laboratory measurements (Fig. 10) suggest critical Stern numbers of 3–16 in conflict with Holyer's (1981) value of 1/3 for low vertical wavenumber instability. One explanation might be that the parasitic instabilities must grow to finite amplitude before they will disrupt the fluxes. With growth rates comparable to fingers, this would allow significant finger growth between the inception of the perturbations and their disruption of the fluxes.

*c. Parameterization.* Gross diffusivities can be determined by normalizing the average fluxes by gradients smoothed over the staircase structure (Fig. 14). For a critical $Ri_f^{-1} = 5$–11 (assuming that buoyancy-flux constrains the model fluxes), the model eddy diffusivity for buoyancy is $\sim -7 \times 10^{-6}$ m$^2$/s. The finger momentum-flux viscosity $(\langle u'w' \rangle / U_z)((L_o + l_i)/l_i) \sim 10^{-5}$ m$^2$/s, where $U_z = 0.4N$ (Table 1), $L_o$ is the layer thickness and $l_i$ is the interface thickness. This is not significantly different from that due to molecular viscosity in agreement with recent laboratory measurements (Ruddick *et al.*, 1989). Since their effect on both momentum and buoyancy (density) is small, salt fingers probably play little role in ocean dynamics.

This is not to say that fingers are unimportant. In the western tropical Altantic east of Barbados, salt-fingering must be maintaining the staircase finestructure; turbulence would smooth steppiness because of its flux ratio greater than one and downgradient buoyancy-flux (Kelley, 1988). While for turbulent mixing the 'eddy' diffusivity $K = e \cdot \epsilon/N^2$ with mixing efficiency $e \leq 0.2$, for salt-fingering $K = [(R_\rho - 1)/(1 - R_F)] \cdot \epsilon/N^2$ with a 'mixing efficiency' $[(R_\rho - 1)/(1 - R_F)]$ of 1–3 (Schmitt,

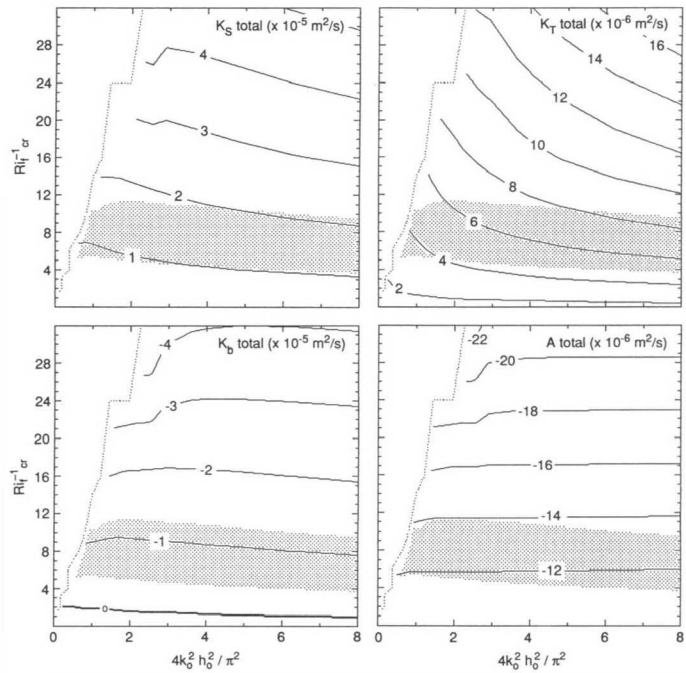


Figure 14. 'Eddy' diffusivities of heat, salt, buoyancy and momentum from fingers and molecular diffusion as a function of initial and critical conditions (see Fig. 13). The stippling corresponds to the domain defined by the C-SALT buoyancy-flux (≡layer dissipation rate).

1988; Hamilton *et al.*, 1989). Therefore, for the same dissipation rate, fingers mix an order of magnitude more efficiently than turbulence. Mack (1989) finds conductivity microstructure occupying 7% of the Sargasso Sea pycnocline, and identifies 75% of this as turbulence and 25% as fingers. The above argument then implies that fingers may be responsible for 3–4 times as much mixing as turbulence. With other sources of mixing weak in the pycnocline (Gregg, 1987; Moum and Osborn, 1986), fingers may be the principal agent for water-mass modification on decadal timescales.

The model's eddy diffusivity for heat ~4–6 × $10^{-6}$ $m^2/s$, is a factor of five greater than molecular diffusion (Fig. 14). The salt diffusivity, ~$10^{-5}$ $m^2/s$, is smaller than the value deduced by Schmitt (1988) using the upper bound of the Cox number estimates (~30; Gregg and Sanford, 1987), but still a factor of three larger than the eddy diffusivity inferred from turbulent dissipation in a diffusively-stable (no fingering) regime with a GM level internal wave field (5 × $10^{-6}$ $m^2/s$, Gregg and Sanford, 1988).

Predicting the staircase layer and interface thicknesses is well beyond the scope of this model. However, with its greater eddy diffusivity of salt than heat, the staircase might be thought of as being in the 'diffusive-instability' regime. If we adopt the Kelley

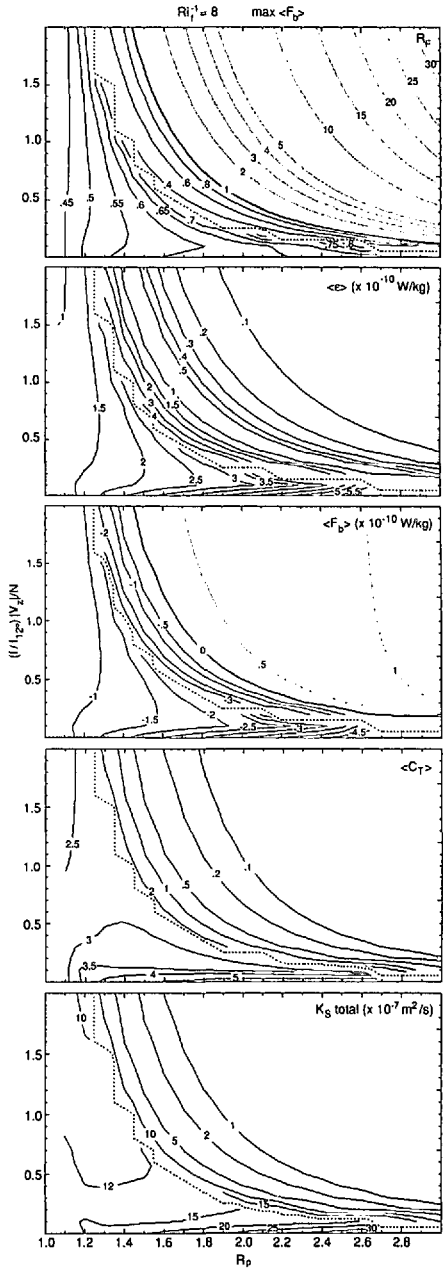


Figure 15. Dependence of the average model flux ratio $R_F$, dissipation rate $\langle\epsilon\rangle$, Cox number $\langle C_T\rangle$, buoyancy-flux $\langle F_b\rangle$ and salt eddy diffusivity $K_S$ on density ratio $R_\rho$ and 'inertial' Froude number for the tilted sheet model. Below and to the left of the thick dotted line, the sheets are constrained by a critical $Ri_f^{-1}$ of eight. To the right and above the thick dotted line, the sheets' $Ri_f^{-1}$ never exceeds eight and the average instead extends to the time of maximum buoyancy-flux. Values may be underestimated at low $R_\rho$ due to the choice of critical $Ri_f^{-1}$. Cox numbers and diffusivities are relative to local (unsmoothed) gradients. For typical ocean shears $\sim 0.7N$, the destabilizing (negative) buoyancy-flux needed to establish and maintain a staircase requires density ratios less than 1.7.

(1984) empirical scaling for the layer thickness applicable for diffusive instability,

$$L_o + l_i = \sqrt{\frac{K_S}{N}} \cdot \left( \frac{0.25 \times 10^9 R_\rho (R_\rho - 1) A}{K_S} \right),$$

applying values typical of the staircase east of Barbados, layer thicknesses of 7–8 m are obtained as compared to the observed 20–30 m layer thicknesses (Boyd and Perkins, 1987). Intriguingly, a value of $K_S$ appropriate for a $\Delta S^{4/3}$ law (which can be thought of as maximal) produces very close agreement between the observed and Kelley layer thickness. This may be because a mixed layer reflects its history, that is, need not be actively mixing. The layer thickness may be a relic of past or sporadic occurrences of high ($\Delta S^{4/3}$) fluxes associated with thin interfaces. Fleury and Lueck (1990) show that at least one interface is occasionally 0.2-m thick.

Finally, at the request of reviewers, we have determined the dependence of the model on the density ratio and shear (Fig. 15). We emphasize that this is premature without a better dynamical understanding of what bounds finger fluxes. Over the timescales that fingers grow, the important shear parameter is its rate of change which depends linearly on $f$ for near-inertial shear. Thus, the vertical axis is a modified Froude number, $(f/f_{12^\circ})(V_z/N)$. Below and to the left of the thick dotted line, the fingers are limited by a constant critical inverse finger Richardson number of 8. Because this constraint does not appear to be universal (Fig. 10), Figure 15 likely underestimates microstructure variances at low density ratio. In addition, the dissipation rates and Cox numbers will be underestimated because the model does not include variance due to parasitic instabilities. Above and to the right of the thick dotted line, sheets never exceed $Ri_f^{-1} = 8$ so averaging runs to the maximum buoyancy-flux. This constraint produces an upper bound for the heat- and salt-fluxes. It is rather arbitrary and results in discontinuities at the boundary, roughly defined by $(f/f_{12^\circ})(V_z/N) = (R_\rho - 1)$, between where the critical $Ri_f^{-1}$ and maximum buoyancy-flux bounds are applied. For $(f/f_{12^\circ})(V_z/N) \lesssim (R_\rho - 1)$, dependence on shear and density ratio is confined within factors of 2–3: the Cox number varies between 2 and 5, the eddy diffusivity of salt between 1–3 $\times$ $10^{-6}$ m$^2$/s, and the dissipation rate between 1–6 $\times$ $10^{-10}$ W/kg. Probably the most important conclusion that might be drawn from Figure 15 is that for typical oceanic shears of $0.7N$, only density ratios less than 1.7 have significant destabilizing (negative) fluxes. This may explain why persistent, well-ordered staircases are only found in regions of low density ratio and weak shear.

*Acknowledgments.* The author gratefully acknowledges the encouragement and insights provided by Melvin Stern, Norge Larson, Dan Kelley, Ray Schmitt and Mike Gregg during the course of this work. The manuscript benefited from careful readings by Dan Kelley, Ray Schmitt, Chris Garrett, Barry Ruddick and Trevor McDougall. The research was supported by NSF contract OCE 86-20101.

## APPENDIX A

**The layer density ratio $R_{\rho L}$ and the flux ratio $R_F$**

Summarized here is McDougall's (1990) argument that the layer density ratio does not constrain the flux ratio because of the nonlinearity of the equation of state. The steadystate equations describing layer property changes in a layer coordinate system are

$$\alpha(V \cdot \nabla_L)\theta + w_i\alpha\theta_z = -\alpha F_{\theta z} \tag{A1}$$

$$\beta(V \cdot \nabla_L)S + w_i\beta S_z = -\beta F_{Sz} \tag{A2}$$

where $\nabla_L$ is the along-layer gradient and $w_i$ is the interface migration (or entrainment) velocity. Defining the *layer density ratio*

$$\boxed{R_{\rho L} = \frac{\alpha(V \cdot \nabla_L)\theta}{\beta(V \cdot \nabla_L)S} = 0.85} \tag{A3}$$

and the *flux divergence ratio*

$$\boxed{R_{Fz} = \frac{\alpha F_{\theta z}}{\beta F_{Sz}},} \tag{A4}$$

(A1) can be expressed

$$R_{\rho L} \cdot \beta(V \cdot \nabla_L)S + R_\rho \cdot w_i\beta S_z = -R_{Fz} \cdot \beta F_{Sz}. \tag{A5}$$

Eliminating the lateral advective term between (A2) and (A5), one arrives at a ratio of the interface migration to the flux divergence for salt

$$\frac{w_i S_z}{F_{Sz}} = -\left(\frac{R_{Fz} - R_{\rho L}}{R_{\rho L} - R_\rho}\right). \tag{A6}$$

Thus, the flux divergence ratio and layer density ratio are not identical as assumed by Schmitt (1988) unless there is no interface migration ($w_i = 0$). Schmitt further assumed that the flux ratio $R_F = \alpha F_\theta/\beta F_S$ and the flux divergence ratio were identical, but this is not the case because of the nonlinearity of the equation of state ($\alpha_\theta = \partial\alpha/\partial\theta \neq 0$). Provided that the flux ratio is invariant with depth

$$\frac{\partial(\alpha F_\theta)/\partial z}{\partial(\beta F_S)/\partial z} = \frac{\alpha F_\theta}{\beta F_S} = R_F. \tag{A7}$$

The coefficient $\alpha$ is not constant but varies significantly with $\theta$ (McDougall, 1987); the variability of $\beta$ is not significant. Therefore, (A7) can be re-expressed

$$\frac{\partial(\alpha F_\theta)/\partial z}{\partial(\beta F_S)/\partial z} = \frac{\alpha F_{\theta z} + \alpha_\theta\theta_z F_\theta}{\beta F_S} = R_{Fz} + R_F \cdot \theta_z\left(\frac{\alpha_\theta}{\alpha}\right)\left(\frac{F_S}{F_{Sz}}\right). \tag{A8}$$

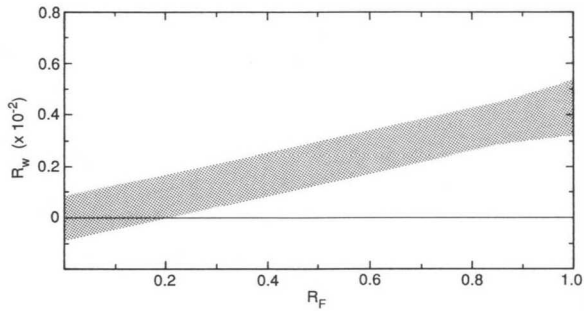


Figure A1. The ratio of the interface migration (entrainment) to finger velocities, $R_w = w_i/w_f$, as a function of flux ratio. The band of stippling covers the range of $\alpha_\theta/\alpha$ and uncertainty in the sign and magnitude of the ratio of the salt-flux divergence to the salt-flux in the staircase east of Barbados. The interface migration velocity is at least two orders of magnitude smaller than the finger velocity.

(A7) and (A8) imply that the flux *divergence* ratio is related to the flux ratio as

$$R_{Fz} = R_F\left[1 - \theta_z\left(\frac{\alpha_\theta}{\alpha}\right)\left(\frac{F_S}{F_{Sz}}\right)\right]. \tag{A9}$$

Substituting the flux divergence ratio (A9) into (A6), one obtains

$$\frac{w_i S_z}{F_S} = \left(\frac{R_{\rho L} - R_F}{R_\rho - R_{\rho L}}\right)\left(\frac{F_{Sz}}{F_S}\right) + \frac{R_F}{R_\rho - R_{\rho L}}\left(\frac{\alpha_\theta}{\alpha}\right)\theta_z. \tag{A10}$$

McDougall (1990) argued that turbulence, vertical variation of the flux ratio, isopycnal mixing and double-diffusive intrusions contributed little or no fluxes. Marmorino (1990) and Fleury and Lueck (1990) have recently shown that turbulence is strong enough to raise the flux ratio from the 0.65 for fastest-growing fingers to 0.85. This implies a ratio of turbulent-to-finger salt-flux of ~0.1, supporting McDougall's claim. Thus, the salt-flux $F_S$ is mostly due to fingering

$$F_S = w_f \delta S \tag{A11}$$

where $\delta S$ is given by $h\overline{S}_z/4$ and $h$ is the finger height (Kunze, 1987). Assuming the flux divergence occurs over the scale of the staircase ($F_{Sz} \sim \pm F_S/(10 \cdot L_o)$ where $L_o$ is the layer thickness), the ratio of interface to finger velocity is given by

$$R_w = \frac{w_i}{w_f} = \pm\left(\frac{R_{\rho L} - R_F}{R_\rho - R_{\rho L}}\right)\left(\frac{h}{80 L_o}\right) + \frac{R_F}{R_\rho - R_{\rho L}}\left(\frac{\alpha_\theta}{\alpha}\right)\left(\frac{h}{4}\right)\theta_z. \tag{A12}$$

For the staircase east of Barbados $R_\rho = 1.6$, $L_o = 20$ m, the interface gradient $\theta_z = \Delta T/l_i = 0.3°\text{C/m}$ (Table 1), $R_{\rho L} = 0.85$ (Schmitt *et al.*, 1987), $\alpha_\theta/\alpha = 0.06$–$0.09$ (McDougall, 1987) and $h \sim 0.3$ m (Kunze, 1987). The only free parameters in (A12) are the velocity ratio $R_w$ and the finger flux ratio $R_F$. Figure A1 displays the dependence of the vertical velocity ratio $R_w$ on the flux ratio $R_F$ within the allowable

range of $\alpha_\theta/\alpha$ and flux divergence. Small interface migration velocities have a large impact on the layer properties because they affect the layer properties directly rather than through divergences as is the case for fluxes (A1, A2). A typical finger velocity is ~0.1 mm/s (Kunze, 1987). Thus, a characteristic interface velocity might be $w_i \sim 4$ cm/day $= 16$ m/yr. This is close to the interfacial velocity inferred from an inversion of the C-SALT CTD data (Lee and Veronis, 1990), however, this same inversion found eddy diffusivities an order of magnitude larger than those inferred from C-SALT microstructure measurements.

## APPENDIX B

### Initial growth

It is not possible to find a similarity solution to (8) valid for all time, since the wavevector deforms continuously (9). However, one can determine the initial growth rate for small perturbations. If it is assumed that $D/Dt = \partial/\partial t + ik_x U = \sigma_o$ is the growth rate, $\delta T = -\overline{T}_z \delta_T h/2$, $\delta S = -\overline{S}_z \delta_S h/2$ and $w = (1/2)Dh/Dt = \sigma_o h/2$ (where $\delta_T$ and $\delta_S$ are the relative temperature and salinity contrasts) following Kunze (1987), then there is a single positive growth rate $\sigma_o$ as a function of wavenumber $k$ and tilt $s$

$$\sigma_o = \frac{1}{4}\left[\kappa_T k^2 + \frac{N^2}{\nu k^2(1+s^2) - sU_z}\right]\cdot\cdot\cdot\cdot$$
$$\cdot\left[\sqrt{1 + \frac{4[g\beta\overline{S}_z(\kappa_T - R_\rho\kappa_S)k^2 - \{\nu k^2(1+s^2) - sU_z\}\kappa_T\kappa_S k^4]}{\{\nu k^2(1+s^2) - sU_z\}[\kappa_T k^2 + \overline{N}^2/\{\nu k^2(1+s^2) - sU_z\}]^2}} - 1\right] \quad \text{(B1)}$$

where the background buoyancy frequency squared $\overline{N}^2 = g\beta\overline{S}_z(R\rho - 1)$ and the *background* density ratio $R\rho = \alpha\overline{T}_z/\beta\overline{S}_z$. While at first glance (B1) appears much more complicated than the unsheared growth rate [see (8) in Kunze, 1987], there are really only two differences. First, because the fingers are tilted, the *total* wavenumber squared $k^2$ is coupled with the molecular viscosities and diffusivities rather than just the horizontal wavenumber squared $k_H^2 = k_x^2 + k_y^2$. Second, $\{\nu k^2(1+s^2) - sU_z\}$ replaces $\nu k_H^2$. If $sU_z$ is negligible, this implies that the effective viscous damping will increase markedly as a finger is tilted both because $k^2$ increases (11) and because of $(1+s^2)$ suppression in the momentum balance (8). The $(1+s^2)$ suppression arises because the component of gravitational acceleration along a tilted finger is reduced.

Note that (B1) hinges on the approximation $w = (1/2)Dh/Dt = \sigma_o h/2$. This is valid for exponential growth with constant growth rate $\sigma_o$ as in the unsheared case, but because $s$ (10) and hence $k$ (11) continuously change in shear, this assumption breaks down. Nevertheless, the dependences of the growth rate (B1) on wavenumber $k$ and tilt $s$ yield some insight so a brief discussion follows.

The growth rate $\sigma_o$ is contoured vs. total wavelength $\lambda = 2\pi/k$ and tilt angle $\theta = \text{Arctan}(s)$ in Fig. B1 for (a) $Ri = 6$ and (b) $Ri = 0.25$. Positive values of $\theta$ correspond to fingers tilting *into* the shear, negative values to fingers tilting *with* the shear. For $Ri = 6$, corresponding to conditions found in the staircase east of Barbados,

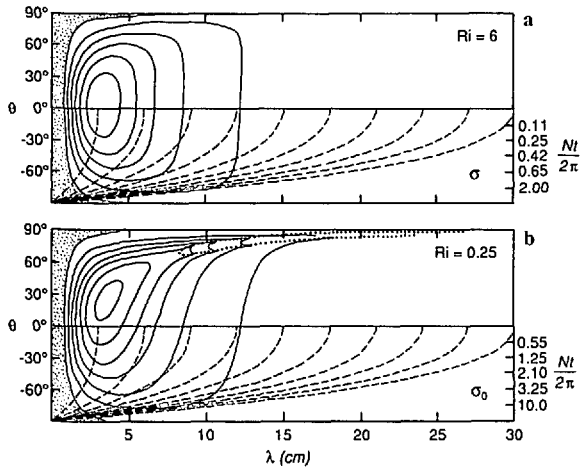


Figure B1. Contours of the real part of the initial growth rate $\sigma_o$ (solid curves) as a function of *total* wavelength $\lambda = 2\pi/k$ and tilt angle $\theta$ = Arctan (s) for square planform ($k_x = k_y$) fingers. Positive $\theta$ corresponds to tilting *into* the shear, negative to tilting *with* the shear. Growth rates are shown for (a) a Richardson number $Ri = 6$ and (b) $Ri = 0.25$. Stippling indicates negative growth rates (decay). For $Ri = 6$, corresponding to conditions found in the staircase east of Barbados, the maximum initial growth rate occurs for vertical fingers ($\theta = 0$) with 3-cm wavelengths. For $Ri = 0.25$, the maximum growth occurs for fingers tilted 30° into the shear. Inside the dotted curve in the upper half of (b), the growth rate has a nonzero imaginary component (implying growing oscillations). The dashed lines describe trajectories of total wavelength $\lambda(t)$ (11) and tilt angle $\theta(t)$ (10) for initially vertical fingers; corresponding times are indicated by the numbers along the right axis. Fingers grow more slowly as they become more tilted.

maximum initial growth corresponds to vertical fingers ($s = k_z = 0$). For $Ri = 0.25$, $sU_z$ is important. Growth rates are faster for moderate tilts *into* the shear because energy for instability can be extracted from the vertical shear as well as the unstable $\overline{S}_z$. Note that these instabilities are *not* classical double-diffusive intrusions because there are no horizontal gradients of temperature and salinity, and *not* McIntyre's (1971) instability because the shear is not geostrophic.

Also plotted in Figure B1 are trajectories (dashed lines) describing the evolution of $\lambda$ (11) and $\theta$ (10) in time for initially vertical ($\theta = k_z = 0$) fingers. The fingers' wavelengths shrink as they tilt progressively *with* the shear. Therefore, a finger that initially has maximal growth rate does not remain fastest-growing. As it is pushed toward higher wavenumber, its growth rate decreases and ultimately goes negative (decay).

## REFERENCES

Batchelor, G. K. 1959. Small-scale variation of convected quantities like temperature in a turbulent fluid. part 1. general discussion and the case of small conductivity. J. Fluid Mech., *5*, 113–133.

Boyd, J. D. and H. Perkins. 1987. Characteristics of thermohaline steps off the northeast coast of South America, July 1983. Deep-Sea Res., *34,* 337–364.

Businger, J. A., J. C. Wyngaard, Y. Izumi and E. F. Bradley. 1971. Flux-profile relationships in the atmospheric surface layer. J. Atmos. Sci., *28,* 181–189.

Caughey, S. J. and S. G. Palmer. 1979. Some aspects of turbulence structure through the depth of the convective boundary layer. Quart. J. Roy. Meteor. Soc., *105,* 811–827.

Chen, C. F. and R. D. Sandford. 1976. Sizes and shapes of salt fingers near the marginal state. J. Fluid Mech., *78,* 601–607.

D'Asaro, E. A. 1984. Wind forced internal waves in the North Pacific and Sargasso Sea. J. Phys. Oceanogr., *14,* 781–794.

—— 1985. Upper ocean temperature structure, inertial currents, and Richardson numbers observed during strong meterological forcing. J. Phys. Oceanogr., *15,* 943–962.

Eriksen, C. C. 1978. Measurements and models of finestructure, internal gravity waves, and wave breaking in the deep ocean. J. Geophys. Res., *83,* 2989–3009.

Evans, D. L. 1981. Velocity shear in a thermohaline staircase. Deep-Sea Res., *28A,* 1409–1415.

Fleury, M. and R. G. Lueck. 1990. Fluxes across a thermohaline staircase. Deep-Sea Res., *37A,* (in press).

Frankignoul, C. J. 1970. The effect of weak shear and rotation on internal waves. Tellus, *22,* 194–203.

Fu, L.-L. 1981. Observations and models of inertial waves in the deep ocean. Rev. Geophys. Space Physics, *19,* 141–170.

Garrett, C., and W. Munk. 1979. Internal waves in the ocean. Ann. Rev. Fluid Mech., *11,* 339–369.

Gregg, M. C. 1987. Diapycnal mixing in the thermocline: A review. J. Geophys. Res., *92,* 5249–5286.

—— 1989. Scaling turbulent dissipation in the thermocline. J. Geophys. Res., *94,* 9686–9698.

Gregg, M. C. and T. B. Sanford. 1987. Shear and turbulence in thermohaline staircases. Deep-Sea Res., *34,* 1689–1696.

—— 1988. The dependence of turbulent dissipation on stratification in a diffusively stable thermocline. J. Geophys. Res., *93,* 12,381–12,392.

Hamilton, J. M., M. R. Lewis and B. R. Ruddick. 1989. Vertical fluxes of nitrate associated with salt fingers in the world's oceans. J. Geophys. Res., *94,* 2137–2145.

Hebert, D. 1988. Estimates of salt-finger fluxes. Deep-Sea Res., *35,* 1887–1901.

Henyey, F. S., J. Wright and S. M. Flatte. 1986. Energy and action flow through the internal wave field: An eikonal approach. J. Geophys. Res., *91,* 8487–8495.

Holyer, J. Y. 1981. On the collective instability of salt fingers. J. Fluid Mech., *110,* 195–207.

—— 1984. The stability of long, steady, two-dimensional fingers. J. Fluid Mech., *147,* 169–185.

Kelley, D. E. 1984. Effective diffusivities within oceanic thermohaline staircases. J. Geophys. Res., *89,* 10,484–10,488.

—— 1988. Explaining effective diffusivities within diffusive oceanic staircases, *in* Small-scale Turbulence and Mixing in the Ocean, J. C. J. Nihoul and B. M. Jamart, eds., Elsevier, The Netherlands, 481–502.

—— 1990. Fluxes through diffusive staircases: A new formulation. J. Geophys. Res., *95,* 3365–3371.

Kunze, E. 1987. Limits on growing, finite-length salt fingers: A Richardson number constraint. J. Mar. Res., *45,* 533–556.

Kunze, E., A. J. Williams III and M. G. Briscoe. 1990. Observations of shear and vertical stability from a neutrally-buoyant float. J. Geophys. Res., *95,* (in press).

Kunze, E., A. J. Williams III and R. W. Schmitt. 1987. Optical microstructure in the thermohaline staircase east of Barbados. Deep-Sea Res., *34*, 1697–1704.

Lee, J. H. and G. Veronis. 1990. On the difference between tracer and geostrophic velocities obtained from C-SALT data. Deep-Sea Res., (submitted).

Lighthill, J. 1978. Waves in Fluids. Cambridge University Press. 504 pp.

Linden, P. F. 1971. Salt fingers in the presence of grid-generated turbulence. J. Fluid Mech., *49*, 611–624.

—— 1973. On the structure of salt fingers. Deep-Sea Res., *20*, 325–340.

—— 1974. Salt fingers in a steady shear flow. Geophys. Fluid Dyn., *6*, 1–27.

Lueck, R. G. 1987. Microstructure measurements in a thermohaline staircase. Deep-Sea Res., *34*, 1677–1688.

Mack, S. A. 1989. Towed-chain measurements of ocean microstructure. J. Phys. Oceanogr., *19*, 1108–1129.

Marmorino, G. O. 1987. Observations of small-scale mixing processes in the seasonal thermocline: Part I: Salt fingering. J. Phys. Oceanogr., *17*, 1339–1347.

—— 1989. Substructure of oceanic salt finger interfaces. J. Geophys. Res., *94*, 4891–4904.

—— 1990. "Turbulent mixing" in a salt-finger staircase. J. Geophys. Res., *95*, 12,983–12, 994.

Marmorino, G. O., W. K. Brown and W. D. Morris. 1987. Two-dimensional temperature structure in the C-SALT thermohaline staircase. Deep-Sea Res., *34*, 1667–1676.

Mazeika, P. A. 1974. Subsurface mixed layers in the northwest tropical Atlantic. J. Phys. Oceanogr., *4*, 446–453.

McDougall, T. J. 1987. Neutral surfaces. J. Phys. Oceanogr., *17*, 1950–1964.

—— 1990. Interfacial advection in the thermohaline staircase east of Barbados. Deep Sea Res., (submitted).

McDougall, T. J. and J. R. Taylor. 1984. Flux measurements across a finger interface at low values of the stability ratio. J. Mar. Res., *42*, 1–14.

McIntyre, M. E. 1970. Diffusive destabilization of the baroclinic circular vortex. Geophys. Fluid Dyn., *1*, 19–57.

Moum, J. N. and T. R. Osborn. 1986. Mixing in the main thermocline. J. Phys. Oceanogr. *16*, 1250–1259.

Oakey, N. S. 1988. Estimates of mixing inferred from temperature and velocity microstructure, *in* Small-Scale Turbulence and Mixing in the Ocean, J. C. J. Nihoul and B. M. Jamart, eds., Elsevier, The Netherlands, 239–247.

Olbers, D. J. 1981. The propagation of internal waves in a geostrophic current. J. Phys. Oceanogr., *11*, 1224–1233.

Osborn, T. R. 1988. Signatures of doubly diffusive convection and turbulence in an intrusive region. J. Phys. Oceanogr., *18*, 145–155.

Phillips, O. M. 1966. The Dynamics of the Upper Ocean. Cambridge University Press, 261 pp.

Piacsek, S. A. and J. Toomre. 1980. Nonlinear evolution and structure of salt fingers, *in* Marine Turbulence, J. C. J. Nihoul, ed., Elsevier, 193–219.

Press, W. H., B. P. Flannery, S. A. Teukolsky and W. T. Vetterling. 1986. Numerical Recipes: the Art of Scientific Computing, Cambridge University Press, 818 pp.

Ruddick, B. R., R. W. Griffiths and G. Symonds. 1989. Frictional stress at a sheared double-diffusive interface. J. Geophys. Res., *94*, 18,161–18,173.

Sanford, T. B. 1975. Observations of the vertical structure of internal waves. J. Geophys. Res., *80*, 3861–3871.

Schmitt, R. W. 1979a. Flux measurements at an interface. J. Mar. Res., *37*, 419–436.

—— 1979b. The growth rate of supercritical salt fingers. Deep-Sea Res., *26A*, 23–44.
—— 1981. Form of the temperature-salinity relationship in the Central Water: Evidence of double-diffusive mixing. J. Phys. Oceanogr., *11*, 1015–1026.
—— 1988. Mixing in a thermohaline staircase, *in* Small-scale Turbulence and Mixing in the Ocean, J. C. J. Nihoul and B. M. Jamart, eds., Elsevier, The Netherlands, 435–452.
Schmitt, R. W. and D. T. Georgi. 1982. Finestructure and microstructure in the North Atlantic Current. J. Mar. Res., *40* (Suppl.), 659–705.
Schmitt, R. W., H. Perkins, J. D. Boyd and M. C. Stalcup. 1987. C-SALT: An investigation of the thermohaline staircase in the western tropical North Atlantic. Deep-Sea Res., *34*, 1655–1666.
Shay, T. J. and M. C. Gregg. 1986. Convectively driven turbulent mixing in the upper ocean. J. Phys. Oceanogr., *16*, 1777–1798.
Shen, C. Y. 1989. The evolution of the double-diffusive instability: salt fingers. Phys. Fluids A, *1*(5), 829–844.
Shirtcliffe, T. G. L. and J. S. Turner. 1970. Observations of the cell structure of salt fingers. J. Fluid Mech., *41*, 707–719.
Simpson, J. H., M. R. Howe, N. C. G. Morris and J. Stratford. 1979. Velocity shear on the steps below the Mediterranean outflow. Deep-Sea Res., *26A*, 1381–1386.
Stern, M E. 1960. The "salt-fountain" and thermohaline convection. Tellus, *12*, 172–175.
—— 1969. Collective instability of salt fingers. J. Fluid Mech., *35*, 209–218.
—— 1975. Ocean Circulation Physics. Academic Press, NY, 191–203.
—— 1976. Maximum buoyancy flux across a salt finger interface. J. Mar. Res., *34*, 95–110.
Stern, M. E. and J. S. Turner. 1969. Salt fingers and convecting layers. Deep-Sea Res., *16*, 497–511.
Taylor, J. and P. Bucens. 1989. Laboratory experiments on the structure of salt fingers. Deep-Sea Res., (submitted).
Taylor, J. and G. Veronis. 1986. Experiment on salt fingers in a Hele Shaw cell. Science, *231*, 39–41.
Turner, J. S. 1967. Salt fingers across a density interface. Deep-Sea Res., *14*, 599–611.
Whitfield, D. W. A., G. Holloway and J. Y. Holyer. 1989. Spectral transform simulations of finite amplitude double-diffusive instabilities in two dimensions. J. Mar. Res., *47*, 241–265.
Williams, A. J. 3rd. 1975. Images of ocean microstructure. Deep-Sea Res., *22*, 811–829.
—— 1981. The role of double diffusion in a Gulf Stream frontal intrusion. J. Geophys. Res., *86*, 1917–1928.

Received: *21 June, 1989;* revised: *10 July, 1990.*